Archaeological and Anthropological Sciences (2023) 15:183
https://doi.org/10.1007/s12520-023-01885-3

RESEARCH

Aqua Alexandrina and Fragole cistern: characterization of mortars from Roman constructions, Rome (Italy)

Laura Calzolari[1] · Laura Medeghini[1,2] · Ilaria Baiocchi[1] · Gian Luca Zanzi[3] · Silvano Mignardi[1,2]

Received: 10 October 2023 / Accepted: 22 October 2023 / Published online: 13 November 2023

Abstract

Aqua Alexandrina is the last aqueduct built by ancient Romans for the city of Rome. At Giovanni Palatucci Park, the archaeological ruins run close to a pre-existent water system, Fragole cistern. This research aims at characterizing mortar samples from both constructions, to identify the materials used and infer about the technological level and the provenance of materials, using a multi-analytical approach. Combining the information obtained through the petrographic investigation of mortar thin sections at optical microscopy and scanning electron microscopy with energy-dispersive X-ray spectroscopy, and X-ray powder diffraction on finely powdered samples and thermogravimetric analysis on the binder fraction, it was possible to attest the presence of both artificial and natural materials with pozzolanic behavior, which conferred hydraulicity to the mortars. The results show that materials are very similar in both constructions, confirming a well-established know-how in the production of hydraulic mortars by the Romans. The volcanic products used as aggregate are identified with two large pyroclastic-flow deposits erupted by the Colli Albani Volcanic District which extensively crop out in the area of Rome: Pozzolane Rosse and Pozzolanelle.

Keywords Hydraulic mortars · Ancient Roman aqueduct · Archaeometric characterization · *Cocciopesto*

Introduction

The supply of water has always been a crucial aspect for ancient Romans, and this is testified by all the network of aqueducts and cisterns that they erected.

In the city of Rome, 11 main aqueducts were erected by Romans. The last one to be built was *Aqua Alexandrina*: it was inaugurated in 226 AD by emperor Severus Alexander (222–235 AD) (Le Pera Buranelli and Turchetti 2007). This aqueduct was *circa* 22 km long, and it got water from the springs located in Pantano Borghese, at 65 m a.s.l., near the 14th mile of ancient Via Prenestina. Its realization was aimed to supply water to a Neronian thermal building located in Campo Marzio near the Pantheon, completely renewed by Severus Alexander in 227 AD (Roncoroni 1972) thanks to whom the name changed in *Thermae Alexandrinae*. The daily flow rate has been estimated to be *circa* 22,000 m^3/day, and because of the thick calcareous concretion still visible today the water should have not been pure enough to be drinkable (Olivos 2014).

The aqueduct is mentioned in late antiquity documents both as *Aqua Alexandrina* (in *Curiosum* and in *De montibus et acquis urbis Romae*) and as *Aqua Alexandriana* (in *Quae sint Romae*); in the tenth century, it was mentioned as *Acqua Iovia* or *forma Iovia*, and this fact has subsequently caused its misinterpretation with *Aqua Antoniniana* (Hostetter et al. 2011; Rustico et al. 2019).

Since its construction, the aqueduct had a troubled life: Thomas Ashby reports lateral inclination of the building, leaks of water, and the addition of a second overlaid *specus* in the stretch of the aqueduct near the spring (Koehler 2017). Ashby identified 435 arches belonging to *Aqua Alexandrina* following the work done by Raffaello Fabretti in the seventeenth century (Fabretti 1680), who firstly recognized the imposing ruins of an aqueduct in Via Prenestina and Via Casilina as part of *Aqua Alexandrina* after the aqueduct oblivion. Unfortunately, the expansion of the residential

✉ Laura Calzolari
laura.calzolari@uniroma1.it

[1] Department of Earth Sciences, Sapienza University of Rome, Piazzale A. Moro, 5-00185, Rome, Italy

[2] CIABC, Sapienza University of Rome, Piazzale A. Moro, 5-00185, Rome, Italy

[3] Sovrintendenza Capitolina ai Beni Culturali, Piazza Lovatelli, 35-00186, Rome, Italy

area and the lack of maintenance in the suburb have caused, in the last centuries, the loss of part of the archaeological remains, with respect to the condition testified by Fabretti and Ashby. The structure was originally made of conglomerate and externally covered by bricks, but already under Diocletian rule there were restoration interventions, such as sustaining intrados. Later in the history of *Aqua Alexandrina*, the earthquake of 394 AD and the barbarian invasions caused several damages to it, and it cannot avoid the faith of all the other aqueducts of Rome (except *Aqua Virgo*), falling into ruin (Deming 2020); however, it is probable that the aqueduct worked until the tenth century, and the presence of defensive towers along its path can suggest postponing its decay until the thirteenth century (Coates-Stephen 1999).

According to archaeological remains still visible today, *Aqua Alexandrina* starts its path East of Rome and reaches the city going West. In Tor Bella Monaca, well-preserved arches are visible, as well as inside the Grande Raccordo Anulare, close to Tenuta Della Mistica, where the *specus* is preserved, but it is in a state of neglect. In Via Walter Tobagi and Via Tor Tre Teste, the aqueduct has overlapped arches. After Giovanni Palatucci Park (also known as Tor Tre Teste Park), the aqueduct's path continues in Via degli Olmi with other restored arches, until the long bridge crossing Viale Palmiro Togliatti, where the aqueduct reaches the maximum height (20.65 m). In the area of Via Casilina, there are no archaeological remains, but they reappear in Via dell'Aquedotto Alessandrino (Koehler 2017). The aqueduct entered Rome through the area called *ad spem veterem*, now Porta Maggiore, and here was located the *piscina limaria*. By now, there are no archaeological remains testifying to the final path of the aqueduct, and several hypotheses have been proposed. Ashby and Fabretti hypothesized a path entering the city from the North, as according to scholars the aqueduct aimed to supply water to *Thermae Alexandrinae* in Campo Marzio, but there are no archaeological remains to support this thesis. Another hypothesis identifies *Aqua Antoniniana* as the final part of *Aqua Alexandrina*, as tracing a hypothetical straight prosecution to the West for this latter aqueduct it meets the ruins of the first one, and also the quotes are compatible (*Aqua Alexandrina* 46 m a.s.l. while *Aqua Antoniniana* 41.6 m a.s.l.) (Koehler 2017). However, *Aqua Antoniniana* is reported to have been built in 213 AD by emperor Caracalla for his Baths, and many scholars consider it a branch of *Aqua Marcia* (Pace 2010; Rustico et al. 2019).

Fragole cistern is located in Giovanni Palatucci Park, close to *Aqua Alexandrina*. Despite the proximity to the aqueduct, the cistern was probably built before it, and it was connected to a suburban *villa*: indeed, the building technique used was the *opus mixtum*, a mix of *opus reticolatum* and *lataericium*, a technique employed between the first and second century AD but not in the third (Vanni 2007).

The current research is focused on the characterization of the hydraulic mortars that constitute the two main archaeological remains in Giovanni Palatucci Park, located in the eastern area of Rome (Fig. 1), which were erected to ensure water supply: *Aqua Alexandrina* and Fragole cistern. For this reason, the research investigated only the mortars from the inner part of the *specus* of the aqueduct and the coating of the internal part of the cistern. The aim is to obtain an archaeometric characterization of the mortars employed in these hydraulic structures to identify the materials used. This is to obtain information on the technological level reached by ancient Romans in the construction of water-resistant systems, to determine if the provenance of the material is local, and eventually compare the mortars from two different structures, both aimed at the supply of water, to highlight differences and similarities.

Brief geological setting

The geological context of the city of Rome is characterized by a large availability of volcanic rocks. This aspect has favored the growth of the city, surely for what concern the building industry, being tuffs largely employed as material for dimension stones and pozzolans particularly suitable as aggregate for mortars and concrete. Giovanni Palatucci Park is located in Municipality 5 of the metropolitan city of Rome. The area East of the Tiber River, in which this district is included, is characterized by a thick succession of pyroclastic-flow deposits from the two main volcanic districts that surround the city, Monti Sabatini and Colli Albani (Funiciello and Giordano 2008). Specifically, the area where the samples were collected is characterized by pyroclastic soils (Cecconi et al. 2010), generated by the activity of Colli Albani Volcanic District, which was formed during the Quaternary, being the main caldera formed 600,000 years ago, and now it is quiescent (Karner et al. 2001; Giordano et al. 2006; Gaeta et al. 2016). The products of the volcanic activity of Colli Albani overly and are in part interbedded with the aggradation successions deposited by the Paleo-Tiber River and its tributaries in response to the glacio-eustatic fluctuations during Middle-Upper Pleistocene (Luberti et al. 2017, and ref. therein). The substrate of these continental successions is constituted by marine clay deposits, Plio-Pleistocene in age ("Monte Vaticano Formation" (Marra and Rosa 1995)). Deep river incisions were originated during the Last Glacial Maximum by coupled regional uplift and sea-level fall, which were successively filled with fluvial sediments at the end of the glacial event (Parotto 2008; Marra et al. 2013). Concerning the effusive and explosive volcanic products, formed during the eruptive activity that took place in the time span 608–36 ka, they both belong to the HK-Series, being the eruptive composition consistently mafic (< 50% SiO_2) (Gaeta et al. 2016). Nonetheless, this

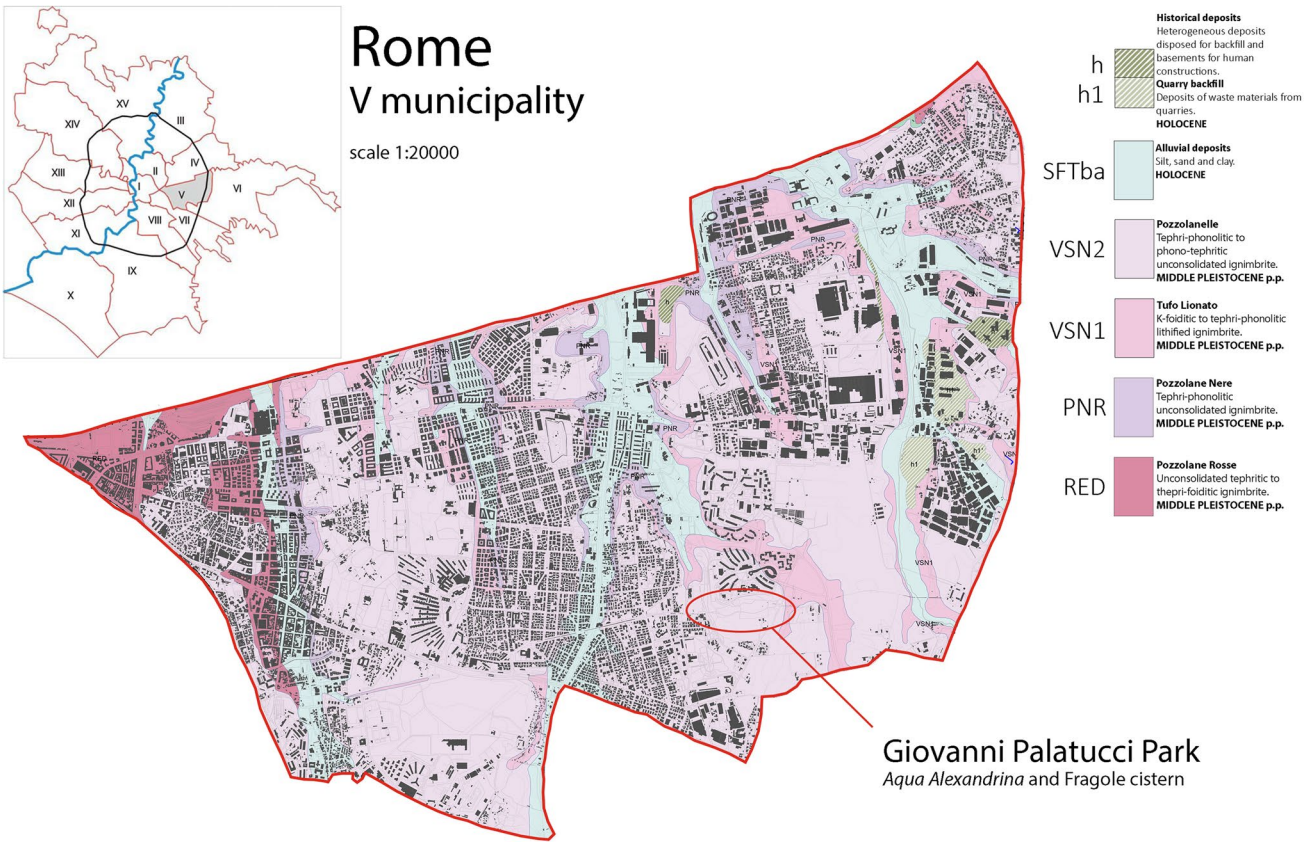

Fig. 1 Geological map of Town Hall 5, modified after Funiciello et al. (2016)

volcano presents the same features of a felsic volcano: low aspect ratio ignimbrites, tens of cubic kilometers large, and a related central collapse caldera (Giordano et al. 2006).

Colli Albani volcano can be divided into four lithosomes, here listed from the oldest to the youngest: Vulcano Laziale lithosome, Tuscolano-Artemisio composite lithosome, Faete lithosome, Via dei Laghi composite lithosome (Funiciello and Giordano 2008).

Vulcano Laziale lithosome was characterized by repeated paroxysmal events, occurring between 608 ka and 355 ka (Karner et al. 2001; Marra et al. 2009; Gaeta et al. 2016). The result is a succession of ignimbrites interbedded with scoria fall deposits, lava flows, and volcanoclastic deposits (Giordano et al. 2006).

Concerning the stratigraphic units outcropping in the area of Municipality 5 (Fig. 1), starting from the oldest ones, there are Pozzolane Rosse, an unconsolidated tephritic to tephri-foiditic ignimbrite (457 ± 4 ka), and Pozzolane Nere, a tephri-phonolitic unconsolidated ignimbrite (407 ± 4 ka), both belonging to the Torrino Synthem (San Palo Formation, Marra and Rosa 1995; Karner and Marra 1998), Middle Pleistocene. Villa Senni Formation (365 ± 4 ka) also characterizes the area: it comprises two eruptive units: Tufo Lionato, a K-foiditic to tephri-phonolitic lithified ignimbrite, and Pozzolanelle, a tephri-phonolitic to phono-tephritic unconsolidated ignimbrite (Freda et al., 1997). Alluvial deposits of silt, sand, and clay, belonging to Fiume Tevere Synthem (Holocene) (Funiciello and Giordano 2008), are also present. Being an anthropic area, heterogeneous deposits disposed for backfill and basements of human construction and deposits of scrap materials from caves are present (Funiciello et al. 2016).

Materials and methods

Samples

Eight mortar/plaster samples were collected at Giovanni Palatucci Park, two from the Fragole cistern (AL4, AL5) and six from *Aqua Alexandrina* (AL6-11). The samples were collected using a chisel and a hammer. The area of sampling

is shown in Fig. 2 and the list of samples is reported in the Supplementary material.

Methods

Each sample firstly underwent a macroscopic analysis, to describe the type of mortar, the presence of altered surfaces, the color (of the binder and of the clasts of aggregate), the dimension of the aggregate, and the cohesion (BENI CULTURALI - NORMAL 2006).

Optical microscopy (OM) on thin sections allowed us to obtain a petrographic characterization of each sample. OM observations were performed using a Leica DM750 P microscope, with video camera Leica MC190 HD and LAS V4 4.12 software, following (Pecchioni et al. 2014).

Part of each sample was finely ground in an agate mortar to perform X-ray powder diffraction (XRPD) analysis to obtain information on the mineralogical phases present both in the binder and in the aggregate. A Bruker D8 focus diffractometer was used, with CuKα radiation, operating at 40 kV and 30 mA. The following instrumental setup was chosen: 3–60° 2θ range and a scan step of 0.02° 2θ/2 s. Data processing, including semiquantitative analysis based on the "Reference Intensity Ration Method," was performed using XPowderX software.

Scanning electron microscopy coupled with energy-dispersive X-ray spectroscopy (SEM-EDS) was performed for the micro-morphological characterization and the micro-chemical analyses. The instrument used is a FEI Quanta 400 scanning electron microscope. Thin sections were previously metallized with graphite and images were collected in back-scattered electrons mode (BSE).

Samples were also analyzed using thermogravimetric analysis (TGA), to estimate the hydraulicity. Samples have been sieved to obtain the fraction most representative of the binder, which in the literature is reported to be the one smaller than 63 µm (Biscontin et al. 2002; Maravelaki-Kalaitzaki et al. 2003). Only samples AL5, AL6, AL7, AL10, and AL11 presented enough material (10–25 mg) for the analysis. The analyses were carried out with a TGA-DSC3+ Mettler Toledo instrument at ISTerre (Grenoble, France), in an N_2 atmosphere, heating the sample from 25 to 1000 °C, with a heating rate of 10 °C/min. Attenuated total reflectance Fourier transform infrared spectroscopy (ATR-FTIR) has been performed on each sample using a Spectrometer FTIR Nicolet iS50 Thermo Scientific (ISTerre, Grenoble, France), before and after TGA, to check the

Fig. 2 Satellite image from Google Earth (04/2022) of Giovanni Palatucci Park, showing the points where the samples were collected. The red circle on the left indicates the Fragole cistern, where samples AL4–AL5 came from. The two red dots indicate the points on the aqueduct, and particularly on the *specus*, where samples AL6–AL9 were collected. The red circle on the right indicates some ruins of *Aqua Alexandrina* that collapsed and are no more in the original configuration; however, it is still possible to recognize the *specus*, and here samples AL10–AL11 were collected

composition before and after the analysis. The spectra were analyzed using OMNIC software.

Results

Macroscopic description

The samples collected from Fragole cistern are both covering layers of the lateral walls. They both present a binder with a light color, almost white. AL4 shows a big ceramic fragment (centimetric dimension) red-orange in color. The rest of the aggregate, fine conglomeratic, is composed of ceramic fragments ochre in color and natural materials dark brown and grey in color. AL5 does not show centimetric ceramic fragments as it is composed of a very fine aggregate fraction. The cohesion is hard in both samples.

Samples from the aqueduct (AL6–AL11) are characterized by a grey/light grey binder. All samples are conglomeratic, with an aggregate constituted by ceramic and rock fragments. AL6 and AL11 show ceramic fragments of centimetric dimension. Lumps can be seen in AL7, AL8, and AL9. All the samples from the aqueduct show a hard cohesion except AL9, which is more friable.

Optical microscopy

The OM investigation is aimed at the characterization of the binder and the finest fraction of the aggregate (Fig. 3). The analyses carried out by OM in the thin sections of each sample showed that all of them present a calcic lime binder, micritic, grey in color. The binder is generally not uniform in texture, with areas of micritic calcite that present different intensities of color. Another common feature of all the samples is the binder-to-aggregate ratio, which is 1:3. Lime lumps are present in all samples, except AL6; in AL9 a relic of limestone has been identified, whereas in AL10 few underburnt marble fragments are present (Fig. 3g–h).

Concerning the aggregate, in all the samples, ceramic fragments have been identified, except for AL8 (which however present them at the macroscopic characterization). The color of the matrix of the ceramic fragment ranges from ochre to red to brown, and the presence of quartz is almost ubiquitous. Some ceramic fragments present pyroclastic rock fragments with porphyritic texture and red color as inclusions. Moreover, in samples AL6 and AL10, it is possible to identify leucite crystals with star-like habit in the pyroclastic rock fragments in the ceramics.

The aggregate is also constituted by pyroclastic rock fragments: this type of aggregate is present in all samples. The color of the matrix ranges from red to brown; the texture is porphyritic; phenocrysts of clinopyroxene, biotite, and leucite are present; pores are mainly small and rounded with secondary crystallizations inside; shape, dimensions, and sphericity are variable. Among these fragments of pyroclastic rock, some with reddish matrix, scarcely porphyritic, and with idiosyncratic leucite crystals with star-like habit have been found in samples AL7, AL8, and AL10, and can be identified as Pozzolane Rosse (D'Ambrosio et al. 2015; Marra et al. 2015, 2016). Glazed pyroclastic rock fragments, with small leucite crystals with star-like habit not homogeneously distributed in the vitreous matrix and elongated and aligned pores, are common among the samples; in AL4, AL7, and AL11, the glass color is darker with respect to AL8 and AL10 where it is yellow. In samples AL8 and AL11, also volcanic rock fragments are present, and they are composed mainly of leucite crystals (100 µm average dimension) with concentric inclusions, prismatic clinopyroxenes brownish and green (smaller than 100 µm), and opaques, in a grey matrix in which crystals are not optically resolvable; this assemblage is ascribable to "Italite," typically occurring in the Pozzolanelle pyroclastic-flow deposit (Freda et al. 1997). A single fragment of holocrystalline rock composed of crystals highly altered, probably ascribable to nepheline, was found in sample AL11. The dimension of the different types of aggregate allows us to define two main groups: a coarse aggregate fraction, in which the aggregate reaches several millimeters in dimension, and a fine aggregate of micrometric dimension. Leucite, amphiboles, and pyroxene as dispersed crystals in the binder are attributable to volcanic rock fragments. They vary in dimensions and quantity among the samples. The presence of aggregates with pozzolanic behavior, i.e., ceramic fragments and pyroclastic rock fragments, induces a reaction with the binder, detectable by the presence of reaction rims around the aggregates and reacted areas in the binder as it looks not homogeneous in color in PPL (plane-polarized light) (Fig. 3i–l).

Pores have different dimensions and shapes with no orientation and non-uniform distribution; the abundance in all the samples ranges from a minimum of 10% to a maximum of 25%, and it is not significative to distinguish among samples.

XRPD

Results of XRPD, performed on each sample, are shown in Table 1. Calcite is ubiquitous among the samples, being abundant in all of them except AL7 and AL8. Clinopyroxene is another ubiquitous phase, detected in all the samples with similar abundance. Felspathoids are present in all the samples, with variable abundances: the presence of leucite is attested in all the samples except AL6, where however analcime is detected, as also in samples AL4, AL7, AL8, and AL9. Biotite has been detected in samples from AL4 to AL9, from scarce to abundant. Feldspar is scarce in samples AL4, AL6, and AL7, and it is present in trace in AL9. Gypsum is present only in AL5 and its presence can be due

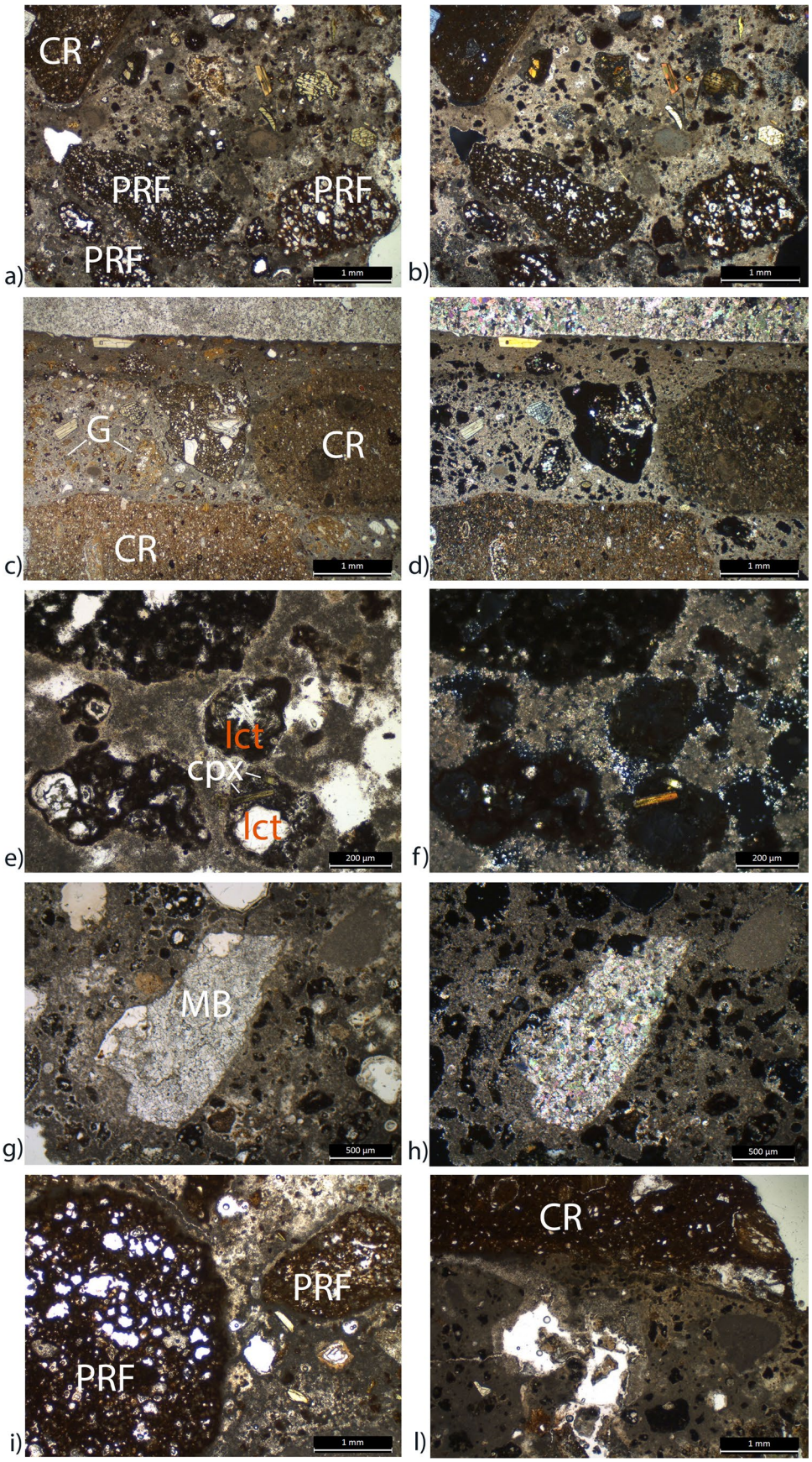

Fig. 3 OM microphotographs of samples from Fragole cistern (**a**, **b**, **i**), and samples from *Aqua Alexandrina* (**c**, **d**, **e**, **f**, **g**, **h**, **l**). Images **a** in PPL (plane-polarized light) and **b** in XPL (cross-polarized light) of sample AL4 show a micritic lime binder not uniform in texture, on top left a fragment of ceramic aggregate (CR), as the rest of the aggregate is composed of pyroclastic rock fragments (PRF), and it is possible to notice the high variability of dimension of the aggregate, as well as the presence of dispersed crystals in the binder. Images **c** in PPL and **d** in XPL of sample AL7 show a stratigraphic section, still presenting on top of the mortar sample the calcareous precipitation due to the water flowing in the duct; the binder looks more compact on top (the most external part of the *cocciopesto* at the base of the duct) rather than on the bottom of the section; big ceramic fragments (CR) mixed with natural materials constitute the aggregate; in the middle of the image and on the left, it is possible to distinguish some glazed pyroclastic rock fragments (G), with small leucite crystals with star-like habit, not homogeneously distributed in the vitreous matrix, which appears ochre at PPL. Images **e** in PPL and **f** in XPL of sample AL10, at higher magnification with respect to the previous ones, show the micrometric fraction of the aggregate, constituted by pyroclastic rock fragments with brown matrix in which leucite (lct) and clinopyroxene (cpx) crystals are distinguishable. Images **g** in PPL and **h** in XPL of sample AL10 show the presence of a marble fragment (MB). Image **i** in PPL from sample AL5 shows the interaction between the pyroclastic aggregate (PRF) and the binder, whereas image **l** in PPL from sample AL11 shows the reaction rim between a ceramic fragment (CR) and the binder

Table 1 Results of XRPD, performed on the whole mortar samples

Sample	Cal	Cpx	Lct	Anl	Bt	Fsp	Gps
AL4	+++	++	+	tr	++	+	
AL5	+++	++	+		+		++
AL6	+++	++		++	++	+	
AL7	++	++	tr	+++	++	+	
AL8	++	++	tr	++	+++		
AL9	+++	++	++	+	+++	tr	
AL10	+++	++	++				
AL11	+++	++	+++				

++++ very abundant, +++ abundant, ++ present, + scarce, tr trace

Cal calcite, *Cpx* clinopyroxene, *Lct* leucite, *Anl* analcime, *Bt* biotite, *Fsp* feldspar, *Gps* gypsum

to the sulphation process reliable with chemical deterioration of the lime-based mortar by sulfuric acid (present in atmospheric water) (Torraca 2009).

SEM-EDS

Thin sections from samples AL4 (from Fragole cistern), AL7, and AL11 (from *Aqua Alexandrina*) have been selected after OM and XRPD investigations to be analyzed at SEM-EDS, to compare mortars representative of the cistern and the aqueduct.

SEM images at high magnification of the samples collected from the aqueduct reveal that they present some inhomogeneity in the binder; moreover, the EDS analysis shows that both samples are characterized by a binder which contains mainly Ca, but in some areas that result in less compact, they are mainly enriched in Si and Al (Fig. 4). This suggests the formation of hydraulic phases, such as C-A-S-H.

Analyses on sample AL4 allowed us to investigate the interface between aggregate with pozzolanic behavior and binder. Artificial material with pozzolanic behavior, here

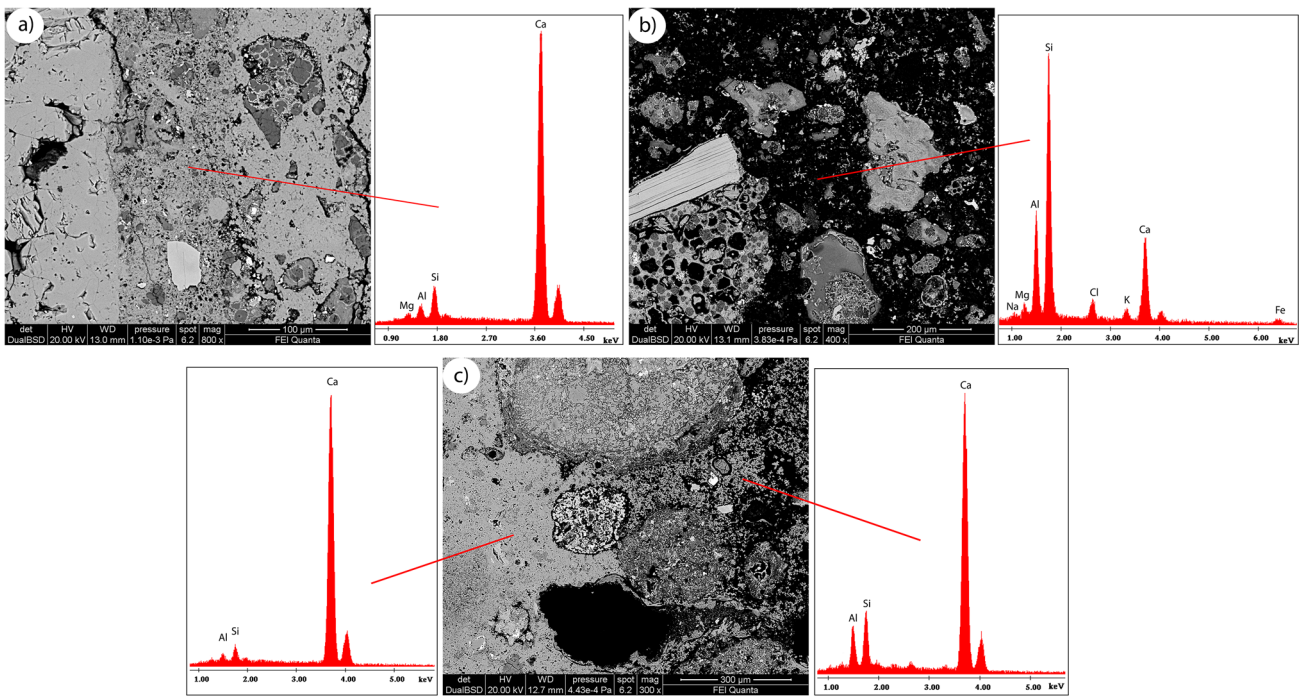

Fig. 4 SEM-EDS analyses on thin sections of sample AL7 and AL11. **a** and **b** show different areas of sample AL7 where the binder has a different composition; in **a**, the most compact area on the left is the carbonatic deposition due to the flow of water, and below the most superficial layer of mortar at the base of the duct is shown; **b** shows an inner area of the same mortar sample, where peaks of Si an Al prevail, suggesting the presence of amorphous hydraulic phases; **c** AL11 showing a non-uniform binder, as testified by the different height of Si and Al peaks

represented by the ceramic fragments of the *cocciopesto*, shows a reaction rim diffused around the aggregate, visually more evident with respect to natural materials with pozzolanic behavior. However, the EDS analyses show that the reaction rim around the ceramic fragment is less enriched in Si, Al, and Mg with respect to the binder area around the volcanic rock fragment, which presents a higher peak of these elements (Fig. 5). In the case of the natural materials with pozzolanic behavior, the exchange of elements between aggregate and binder seems more widespread, and not strictly located around the aggregate fragment, as it is in the case of ceramic.

Concerning the aggregate, the presence of Pozzolane Rosse has been inferred in samples AL7, as at OM, it shows the presence of pyroclastic rock fragments less porphyritic than other rock fragments constituting the aggregate, with abundant leucite crystals with the typical star-like habit. The SEM observations showed the presence of crystals with star-like habit not only in the aggregate of AL7, but also in AL4 (Fig. 6a and b); the EDS analyses performed on the star-like crystals detected the presence (in order of abundance) of Si, Al, and Na; as K, the major component of leucite, is not present, analcimization has occurred, substituting it with Na and producing analcime. This phenomenon has been attested also in other Roman mortars containing Pozzolane Rosse aggregate (Jackson et al. 2011), and in particular it interests the smallest leucite crystals, which easier underwent substitution by analcime.

Pyroclastic rock fragments with a porphyritic texture have been identified in all the samples. In sample AL4, the phenocrysts found in the pyroclastic rock fragments are micas, clinopyroxenes, leucite, and apatite. In the porosities, acicular crystals with random orientation have been analyzed with EDS, revealing the presence of Ca (Fig. 7a). In AL7, the crystallizations found in the porosities of pyroclastic rock fragments are composed of Al, Si, and Ca (and very few K and Na), as result of the interaction between the pozzolan aggregate and the calcic binder (Fig. 7b). AL11 presents

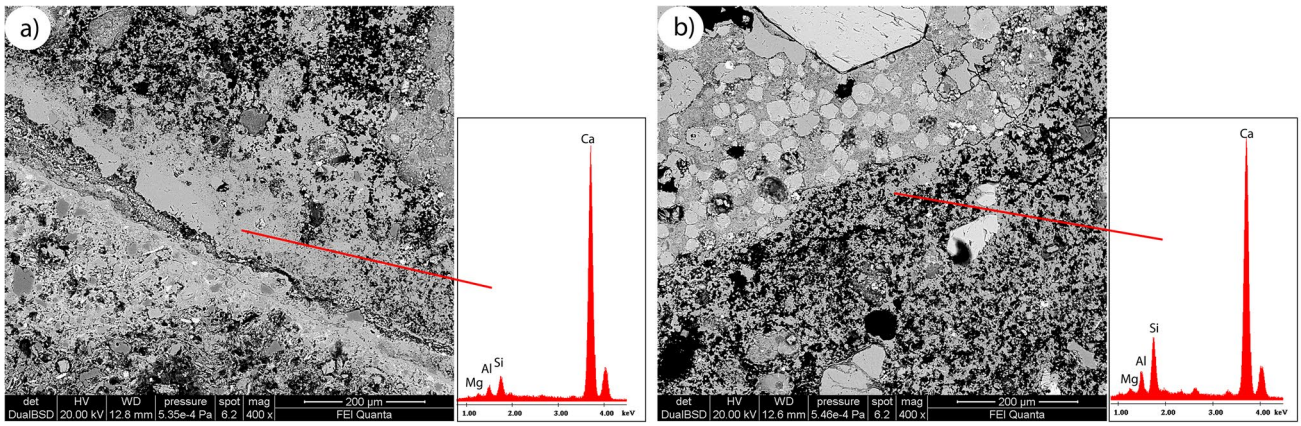

Fig. 5 SEM-EDS analyses on sample AL4. Comparison among **a** interface between a ceramic fragment and the binder, and **b** interface between a volcanic rock fragment and the binder. Despite the fact that visually the reaction rim is more evident in **a**, the area at the interface that results more enriched in Si and Al, suggesting that a hydraulic reaction occurred, is the one shown in **b**

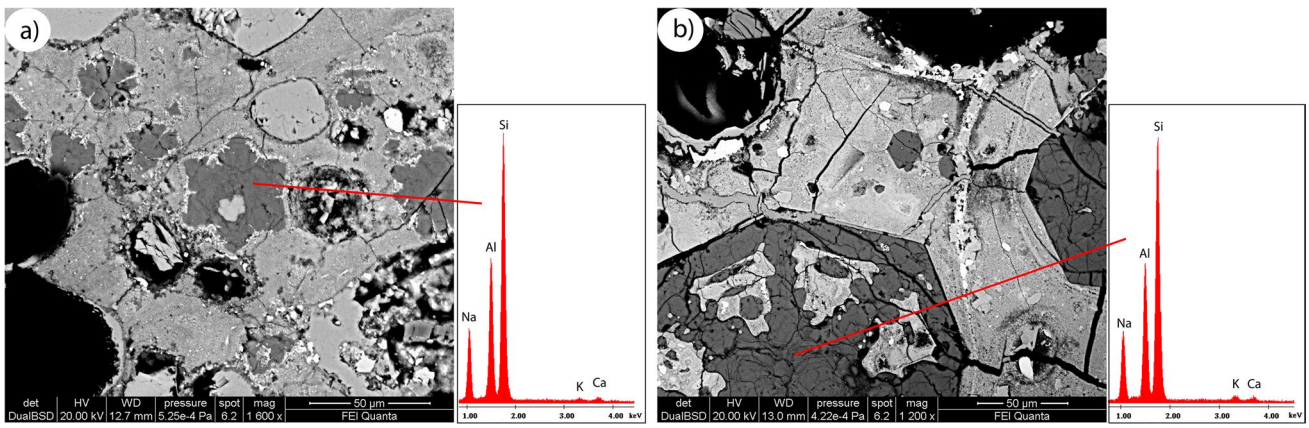

Fig. 6 SEM-EDS analyses on analcimized leucite with star-like habit, typical of Pozzolane Rosse, **a** in sample AL4 and **b** in sample AL7

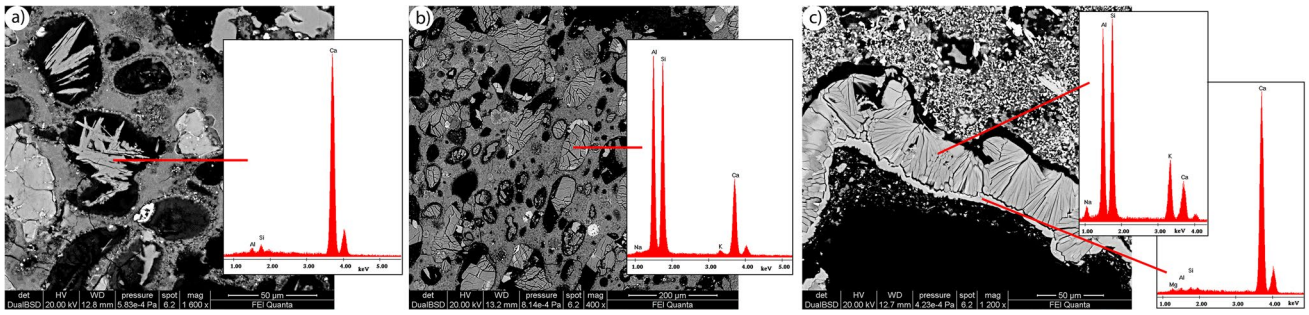

Fig. 7 SEM-EDS analyses on pores filling. **a** Sample AL4 shows acicular crystals rich in Ca filling the pores of the pyroclastic aggregate; **b** sample AL7 presents more compact crystallizations in the pores of the aggregate, composed of Si, Al, Ca, K, and Na; **c** sample AL11 shows in the inner part of the aggregate's pore elongated crystals with radial disposition, composed of Si, Al, K, Ca, and Na, covered on top with a Ca-rich layer

crystallization in the pores of pyroclastic rock fragments that are more complex (Fig. 7c): elongated crystals with radial disposition are covered on top by a thin stratum of different composition. The radial crystals are composed of Si, Al, K, Ca, and Na, which is compatible with the composition of zeolite crystals, whereas the covering layer is rich in Ca and is probably a secondary crystallization of calcite. The matrix of the pyroclastic rock fragments found in all the three samples is similar, being composed (in order of intensity of the peaks) of Si, Al, Ca, Na, Mg, Fe, K, and Ti.

In sample AL11, also a holocrystalline rock fragment has been found (Fig. 8a); as described at OM, it is mainly composed of large anorthoclase and nepheline crystals, which are accompanied by areas that result white at SEM, with irregular shape and a net structure. The EDS spectra on these white areas show the presence (in order of intensity of the peaks) of Si, Ca, Mg, Al, Fe, K, Na, Mn, and Ti.

Ceramic fragments used as an aggregate have been analyzed in sample AL4 (Fig. 8b). The composition of the matrix is rich in Si, followed by Al and Ca, and minor content of Mg, K, Fe, Na, Ti, and S. The crystals present in the ceramic fragments are mainly represented by quartz and anorthoclase.

Thermogravimetric analysis

The binder of samples AL5 (Fragole cistern) and AL6, AL7, AL10, and AL11 (*Aqua Alexandrina*) underwent thermogravimetric analysis, to evaluate the hydraulicity of the mortar (Moropoulou et al. 2004). As shown in the diagram (Fig. 9), all the samples had a similar behavior, but a different percentage of weight loss above 600 °C, which indicates a difference in the content of carbonate phases. The presence of carbonates is confirmed also by ATR analyses (peaks at 1405, 875, and 712 cm^{-1}). The peaks representative of these phases disappear or change in intensity and shape in the samples analyzed after TGA, as well as the peak of water between 3000 and 3600 cm^{-1} disappears (Fig. 10). In order to evaluate hydraulicity, the CO_2/H_2O ratio has been calculated: this ratio is used to evaluate the degree of hydraulicity because it takes into account the weight loss due to the decomposition of carbonate phases (over 600 °C) and the loss of water bond to hydraulic compounds (200–600 °C) (Elsen et al. 2012). The values of the CO_2/H_2O ratio are reported in Table 2. The closest the value is to zero, the highest is the hydraulicity. It is interesting to note that even if sample AL5 presents a relevant weight loss above 600 °C, as it has also a consistent weight loss between 200 and 600 °C, it is the second in content of hydraulic phases. The values of the CO_2/H_2O ratio of all samples confirm the hydraulic nature of all the mortars (Moropoulou et al. 1995).

Discussion

The multi-analytical approach used for the characterization of mortars and plaster from Fragole cistern and *Aqua Alexandrina* at Giovani Palatucci Park, comprehensive of OM, XRPD, SEM-EDS analyses, and TGA, allows to define the analyzed samples as hydraulic mortars, because of the presence of both artificial and natural materials with pozzolanic behavior. Their presence enhanced the hydraulic reaction in the binder, and this is testified by SEM-EDS analyses carried on the binder and on the reaction rims showing an increase in Si and Al content in the Ca-rich binder, and also by CO_2/H_2O ratio values that confirm the hydraulic nature of the mortars. In fact, ancient Romans were used to mix a calcic lime binder, which by itself is aerial and it is able to settle only in the presence of air, with aggregate materials that enrich the system in Si and Al, favoring the hydraulic reaction (Torraca 2009; Pecchioni et al. 2018; Ranieri et al. 2018; Secco et al. 2020).

Indeed, pyroclastic rock and glazed rock fragments are present as aggregate in all the samples. These materials

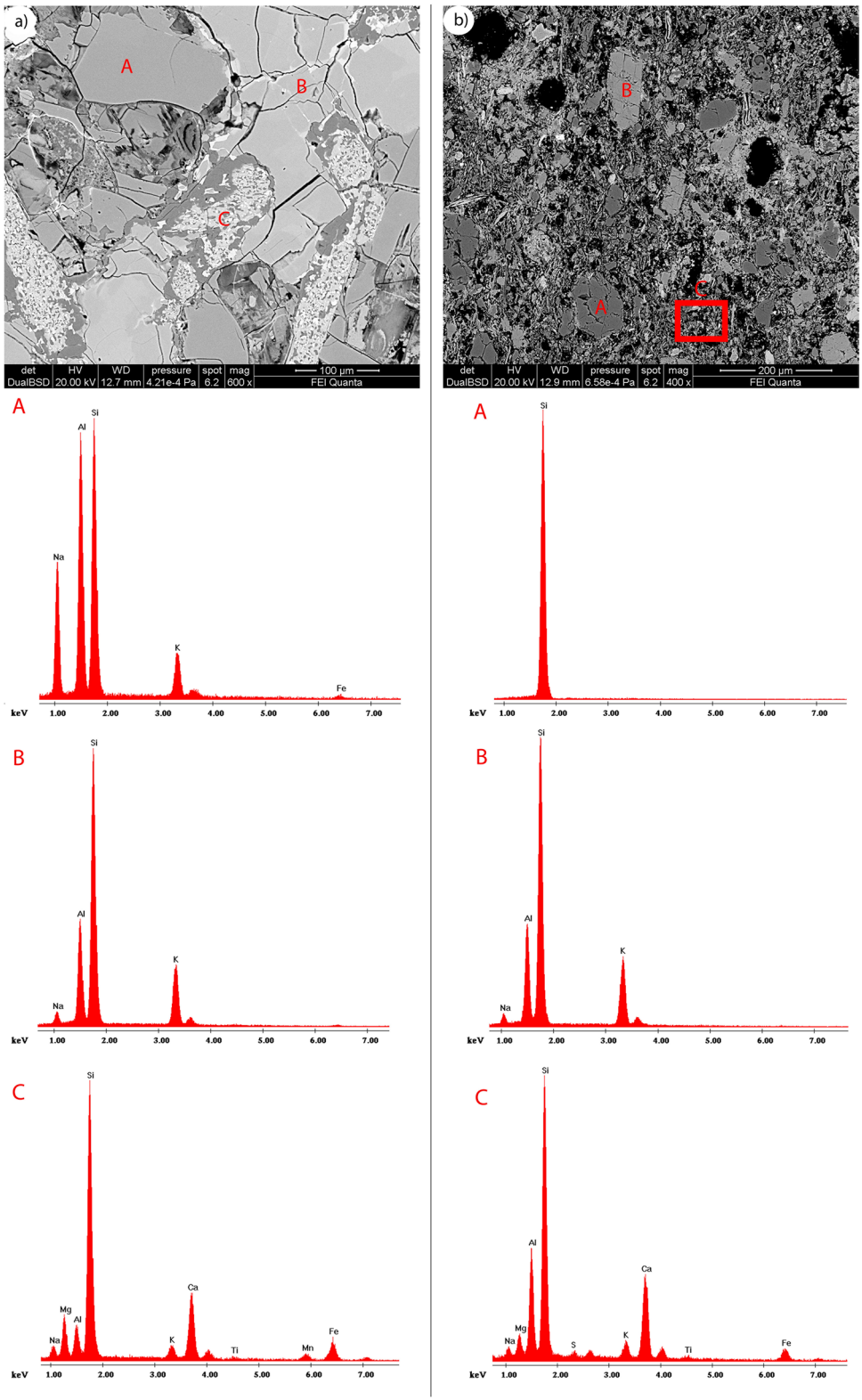

Fig. 8 SEM-EDS analysis on thin sections. **a** Holocrystalline rock fragment in AL11, with a chemical composition compatible to nepheline (point A) and anorthoclase (point B), a white net area composed of Si, Ca, Mg, Al, Fe, K, Na, Mn, and Ti (point C); **b** ceramic fragment in AL4, presenting quartz (point A), anorthoclase (point B), and a matrix composed of Si, Al, Ca, and minor content of Mg, K, Fe, Na, Ti, and S (area C)

are fundamental as the amorphous silica and alumina react with water and lime to form hydrated calcium silicates and hydrated calcium aluminates which provide resistance and strength to the mortar. OM analyses showed inhomogeneity in the binder, and this was confirmed by SEM-EDS analyses, which showed areas enriched in Si and Al, especially close to the type of aggregate just described above, which is in agreement with previous studies attesting that the presence

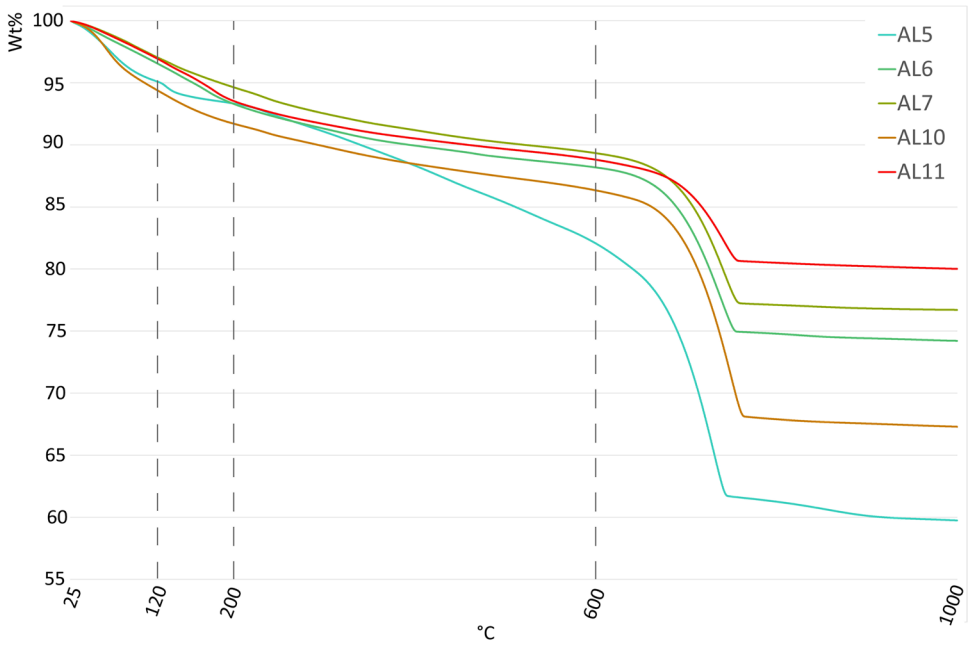

Fig. 9 TGA diagram showing the weight loss of the binder fraction of samples AL5 (Fragole cistern) and AL6, AL7, AL10, and AL11 (*Aqua Alexandrina*). The main intervals of interest are delineated in the diagram: below 120 °C, the sample is characterized by the loss of adsorbed water, between 200 and 600 °C, the loss of water from hydraulic phases occurs, and above 600 °C, the weight loss is related to the decomposition of carbonate phases

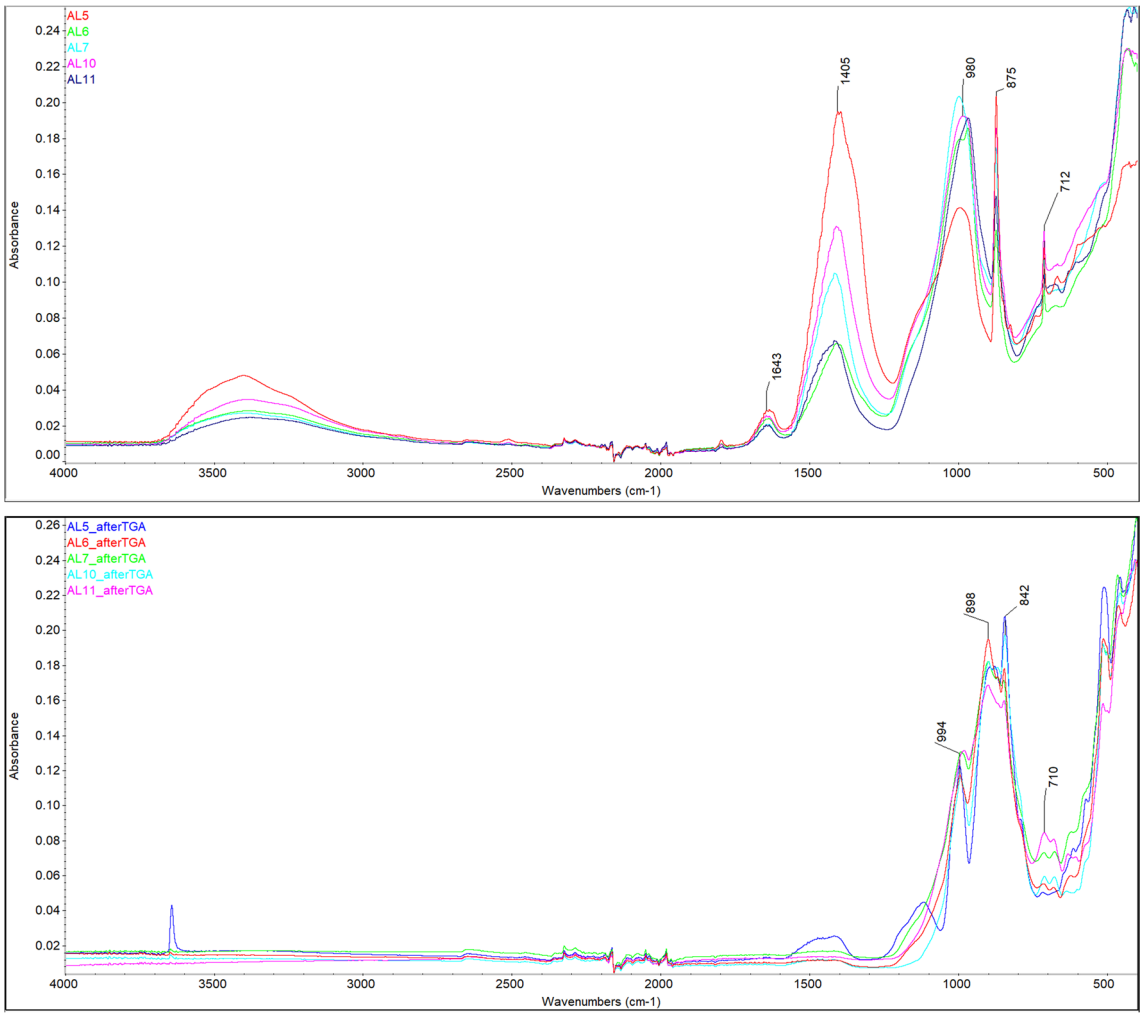

Fig. 10 ATR analyses on the samples, before (top) and after (bottom) TGA

Table 2 Calculation of the CO_2/H_2O ratio. The closest the value is to 0, the highest is the hydraulicity

Sample	Weight loss in each temperature range (°C)				CO_2/H_2O
	<120	120–200	200–600	>600	
AL5	4.88	1.73	11.21	22.43	2.00
AL6	3.40	3.15	5.23	14.00	2.68
AL7	2.92	2.33	5.39	12.66	2.35
AL10	5.56	2.63	5.43	19.09	3.51
AL11	3.01	3.30	4.84	8.83	1.82

of natural pozzolanic materials produces more hydraulic mortars than artificial pozzolanic materials (Moropoulou et al. 2004, 2005).

Furthermore, the presence of ceramic fragments is due to their pozzolanic behavior. Ancient Romans used a technique called *cocciopesto* whenever a masonry would be in contact with water. A wide discussion in the field of archaeology interests the correct definition of *cocciopesto*, and its comparison with what is called *opus signinum*. The majority of scholars now agree that the term *opus signinum* (i.e., "structure made in the way used in *Signa*", today Segni, a city located south-east of Rome) refers to a mural or paving coarse rubble structure, used in hydraulic systems, whereas *cocciopesto* refers to a mural or paving covering layer (Cifarelli et al. 2017; Giuliani 2018). As reported in the Supplementary material, the samples analyzed in this study have different functions: the ones coming from the Fragole cistern are both covering layers of the lateral walls (AL4, AL5), the samples coming from the aqueducts are thick layers of mortar at the base of the specus (AL6, AL8, AL11), lateral borders connecting the base of the specus with lateral walls (AL7, AL10), and one is a mortar collected between bricks, under the specus (AL9). Despite the different displacements of the mortar and the difference in the dimension of the biggest fraction of the aggregate, which is mainly represented by ceramic fragments, the finest fraction looks similar in all the samples, being characterized by the presence of pyroclastic rock fragments.

The binder of the samples is a calcic lime, with grey color and non-homogeneous texture. The presence of underburnt lumps in the samples could suggest a not optimal calcination of the limestone, related to the inhomogeneous distribution of the temperature in the kiln. In addition, the identification of few marble fragments at OM in sample AL10 can suggest the use of this material to produce the binder, at least in this sample. Marble is in fact one of the stones advised in Roman times for lime making (Pavía and Caro 2008).

The mortars from Fragole cistern and *Aqua Alexandrina* do not show main differences even after this archaeometric investigation, suggesting that even if the two structures have never been connected and were not built in the same period (Vanni 2007), the masonry technique used by ancient Romans for structures in contact with water followed a well-known and established procedure.

Concerning the provenance of the natural pozzolanic materials, the results of the petrographic analyses evidence idiosyncratic features allowing for the identification of the Colli Albani eruptive products as the main constituent of the aggregates. Indeed, these products range from K-foidite to tephrite and tephri-phonolite and are characterized by the absence of sanidine and plagioclase and a modal assemblage consisting of leucite and clinopyroxene (biotite is accessory) (Marra et al. 2011). In particular, samples AL4, AL7, AL8, and AL10 are characterized by the occurrence of glassy aggregate fragments, with small leucite crystals displaying star-like habit not homogeneously distributed in the vitreous matrix, which have been attested in Colli Albani volcanic products such as Pozzolane Rosse (Marra et al. 2022) and Tufo del Palatino (Gaeta et al. 2021). Furthermore, the presence in samples AL8 and AL11 of holocrystalline aggregate fragments, constituted by leucite, clinopyroxene, and opaques ("Italite"), is typical of the Pozzolanelle pyroclastic-flow deposit (Freda et al. 1997; Marra et al. 2016).

Results of our study, showing the jointed use of Pozzolane Rosse and Pozzolanelle in the investigated third-century aqueduct, confirm and provide new insights on the timeline of employment of local pozzolanic materials in Roman architecture. Indeed, the Pozzolane Rosse is the material that ancient Romans preferred in mortar formulation in this area since the end of the second century BC and it was integrated by the Pozzolanelle at the passage between the second and the third century AD (Marra et al. 2016).

Conclusions

This is the first archaeometric study which compares mortars from Fragole cistern and *Aqua Alexandrina* in the area of Giovanni Palatucci Park.

The multi-analytical approach proposed allowed us to obtain a characterization of the materials constituting the binder, the aggregate, and the interactions that occurred between them. All the samples are hydraulic mortars, in which the hydraulicity is due to the presence of an aggregate with pozzolanic behavior, both artificial and natural.

Despite the differences in the intended use, all the samples present a fine fraction of aggregate constituted by pyroclastic rock fragments. The presence of this fine fraction enhances the hydraulic reaction between aggregate and binder.

Even if the two structures have not been built in the same moment, as testified by archaeological evidence, the mortars are similar, confirming a well-established know-how in the mortar production in the Roman period.

Finally, this multi-analytical characterization evidences a local provenance for the raw materials constituting the aggregate of natural origin, belonging to the Pozzolane Rosse and Pozzolanelle pyroclastic-flow deposits erupted by the Colli Albani Volcanic District.

Supplementary Information The online version contains supplementary material available at https://doi.org/10.1007/s12520-023-01885-3.

Acknowledgements The authors want to express their gratitude to Sovrintendenza Capitolina ai Beni Culturali, and to Soprintendenza Speciale Archeologia, Belle Arti e Paesaggio di Roma, for the authorization to sampling.

Author contribution L. C.: Conceptualization, Data curation, Formal analysis, Investigation, Writing - Original Draft. L. M.: Formal analysis, Writing - review & editing. I. B.: Data curation, Formal analysis, Writing - Original Draft. G.L. Z.: Writing - review & editing. S. M.: Formal analysis, Writing - review & editing.

Funding Open access funding provided by Università degli Studi di Roma La Sapienza within the CRUI-CARE Agreement. This work was supported by Distretto Tecnologico Beni e Attività Culturali – DTC Lazio and Lazio Innova DTC ON-TECH prot. n. 305-2020-35553 del 20/05/2020 with det. G07413 in 16/06/2021 CUP F85F21001090003.

References

BENI CULTURALI - NORMAL (2006) UNI 11176:2006 Cultural heritage - Petrographic description of a mortar

Biscontin G, Birelli MP, Zendri E (2002) Characterization of binders employed in the manufacture of Venetian historical mortars. Journal of Cultural Heritage 3:31–37

Cecconi M, Scarapazzi M, Viggiani G (2010) On the geology and the geotechnical properties of pyroclastic flow deposits of the Colli Albani. Bulletin of Engineering Geology and the Environment 69:185–206

Cifarelli FM, Colaiacomo F, Kay S, et al (2017) The origins of opera signina: the large pool at Prato Felici from the Segni Project excavations. Atti del convegno nazionale "Tecnica di idraulica antica" 163–166

Coates-Stephen R (1999) Le ricostruzioni altomedievali delle Mura Aureliane e degli acquedotti. Mélanges de l'Ecole française de Rome. Moyen-Age:209–225

D'Ambrosio E, Marra F, Cavallo A et al (2015) Provenance materials for Vitruvius' harenae fossiciae and pulvis puteolanis: geochemical signature and historical–archaeological implications. J Archaeolog Sci: Rep 2:186–203

Deming D (2020) The aqueducts and water supply of Ancient Rome. Ground Water 58:152–161. https://doi.org/10.1111/gwat.12958

Elsen J, Van Balen K, Mertens G (2012) Hydraulicity in historic lime mortars: a review. In: Válek J, Hughes JJ, Groot CJWP (eds) Historic Mortars. Springer Netherlands, Dordrecht, pp 125–139

Fabretti R (1680) De aquis et aquaeductibus veteris Romae dissertationes tres. Ioannis Baptistae Bussotti, Roma

Freda C, Gaeta M, Palladino DM, Trigila R (1997) The Villa Senni Eruption (Alban Hills, central Italy): the role of H2O and CO2 on the magma chamber evolution and on the eruptive scenario. J Volcanolog and Geothermal Res 78:103–120. https://doi.org/10.1016/S0377-0273(97)00007-3

Funiciello R, Giordano G (2008) La nuova carta geologica di Roma: litostratigrafia e organizzazione stratigrafica. La geologia di Roma dal centro storico alla periferia Memorie Descrittive della Carta Geologica d'Italia 80:39–85

Funiciello R, Giordano G, Mattei M (2016) Piano regolatore generale, Carta geolitologica del territorio di Roma Capitale, approvato con Del. C.C. n. 18 del 12 febbraio 2008

Gaeta M, Bonechi B, Marra F, Perinelli C (2021) Uncommon K-foiditic magmas: the case study of Tufo del Palatino (Colli Albani Volcanic District, Italy). Lithos 396–397:106239. https://doi.org/10.1016/j.lithos.2021.106239

Gaeta M, Freda C, Marra F et al (2016) Paleozoic metasomatism at the origin of Mediterranean ultrapotassic magmas: constraints from time-dependent geochemistry of Colli Albani volcanic products (Central Italy). Lithos 244:151–164

Giordano G, De Benedetti AA, Diana A et al (2006) The Colli Albani mafic caldera (Roma, Italy): stratigraphy, structure and petrology. J Volcanol Geothermal Res 155:49–80

Giuliani FC (2018) L'edilizia nell'antichità. Carrocci editore, Roma

Hostetter E, Fouke BW, Lundstrom CC (2011) The last flow of water to, and through, the Baths of Caracalla: age, temperature and chemistry. J Anc Topogr Riv Topogr Antica 21:53–90

Jackson MD, Ciancio Rossetto P, Kosso CK et al (2011) Building materials of the theatre of Marcellus, Rome. Archaeometry 53:728–742

Karner DB, Marra F (1998) Correlation of fluviodeltaic aggradational sections with glacial climate history: a revision of the Pleistocene stratigraphy of Rome. Geolog Soc Ame Bull 110:748–758

Karner DB, Marra F, Renne PR (2001) The history of the Monti Sabatini and Alban Hills volcanoes: groundwork for assessing volcanic-tectonic hazards for Rome. J Volcanol Geothermal Res 107:185–219

Koehler J (2017) L' Acquedotto Alessandrino. Ricerche sull' ultimo acquedotto della Roma antica. Geologia Dell'ambiente 3:223–225

Le Pera BS, Turchetti R (2007) I giganti dell'acqua: acquedotti romani del Lazio nelle fotografie di Thomas Ashby : 1892-1925. Palombi

Luberti GM, Marra F, Florindo F (2017) A review of the stratigraphy of Rome (Italy) according to geochronologically and paleomagnetically constrained aggradational successions, glacio-eustatic forcing and volcano-tectonic processes. Quaternary Int 438:40–67

Maravelaki-Kalaitzaki P, Bakolas A, Moropoulou A (2003) Physico-chemical study of Cretan ancient mortars. Cement Concrete Res 33:651–661. https://doi.org/10.1016/S0008-8846(02)01030-X

Marra F, Bozzano F, Cinti FR (2013) Chronostratigraphic and lithologic features of the Tiber River sediments (Rome, Italy): implications on the post-glacial sea-level rise and Holocene climate. Global Planet Change 107:157–176

Marra F, D'Ambrosio E, Gaeta M, Mattei M (2016) Petrochemical identification and insights on chronological employment of the volcanic aggregates used in Ancient Roman mortars. Archaeometry 58:177–200. https://doi.org/10.1111/arcm.12154

Marra F, D'Ambrosio E, Gaeta M, Monterroso-Checa A (2022) Petrographical and geochemical criteria for a chronology of Roman mortars between the first century BCE and the second century

CE: the Curia of Pompey the Great. Archaeometry 64:597–610. https://doi.org/10.1111/arcm.12740
Marra F, Danti A, Gaeta M (2015) The volcanic aggregate of ancient Roman mortars from the Capitoline Hill: petrographic criteria for identification of Rome's "pozzolans" and historical implications. J Volcanol Geothermal Res 308:113–126
Marra F, Deocampo D, Jackson MD, Ventura G (2011) The Alban Hills and Monti Sabatini volcanic products used in ancient Roman masonry (Italy): an integrated stratigraphic, archaeological, environmental and geochemical approach. Earth-Sci Rev 108:115–136. https://doi.org/10.1016/j.earscirev.2011.06.005
Marra F, Karner DB, Freda C et al (2009) Large mafic eruptions at Alban Hills Volcanic District (Central Italy): chronostratigraphy, petrography and eruptive behavior. J Volcanol Geothermal Res 179:217–232
Marra F, Rosa C (1995) Stratigrafia e assetto geologico dell'area romana. Memorie Descrittive della Carta Geologica d'Italia 50:49–118
Moropoulou A, Bakolas A, Aggelakopoulou E (2004) Evaluation of pozzolanic activity of natural and artificial pozzolans by thermal analysis. Thermochimica Acta 420:135–140. https://doi.org/10.1016/j.tca.2003.11.059
Moropoulou A, Bakolas A, Anagnostopoulou S (2005) Composite materials in ancient structures. Cement Concrete Composites 27:295–300. https://doi.org/10.1016/j.cemconcomp.2004.02.018
Moropoulou A, Bakolas A, Bisbikou K (1995) Characterization of ancient, byzantine and later historic mortars by thermal and X-ray diffraction techniques. Thermochimica Acta 269–270:779–795. https://doi.org/10.1016/0040-6031(95)02571-5
Olivos JMDLP (2014) El último gran acueducto de Roma: Aqua Alexandrina (siguiendo los pasos de Fabretti y Ashby). Revista Digital del Cedex:65–65
Pace P (2010) Acquedotti di Roma e il De aquaeductu di Frontino, 3rd edn Consiglio Nazionale delle Ricerche
Parotto M (2008) Evoluzione paleogeografica dell'area romana: una breve sintesi. In: La Geologia Di Roma Dal Centro Storico Alla Periferia, Memorie Descrittive Della Carta Geologica d'Italia, pp 25–38
Pavía S, Caro S (2008) An investigation of Roman mortar technology through the petrographic analysis of archaeological material. Constr Build Materials 22:1807–1811. https://doi.org/10.1016/j.conbuildmat.2007.05.003
Pecchioni E, Fratini F, Cantisani E (2014) Atlante delle malte antiche in sezione sottile al microscopio ottico. Nardini Editore
Pecchioni E, Fratini F, Cantisani E (2018) Le malte antiche e moderne tra tradizione ed innovazione. Nuova ediz, Pàtron
Ranieri S, Pagnotta S, Lezzerini M et al (2018) Examining the reactivity of volcanic ash in ancient mortars by using a microchemical approach. Mediterranean Archaeol Archaeom Int Sci J 18:147–157
Roncoroni F (tran) (1972) Storia augusta. Rusconi Editore, Milano
Rustico L, Buonfiglio M, Zanzi GL, et al (2019) Viale Guido Baccelli, largo Enzo Fioritto, viale Giotto. Rinvenimento di una diramazione dell'Acquedotto Antoniniano. Bullettino della Commissione Archeologica Comunale di Roma 120:359–364
Secco M, Dilaria S, Bonetto J et al (2020) Technological transfers in the Mediterranean on the verge of romanization: insights from the waterproofing renders of Nora (Sardinia, Italy). J Cult Heritage 44:63–82. https://doi.org/10.1016/j.culher.2020.01.010
Torraca G (2009) Lectures on materials science for architectural conservation. Getty Conservation Institute
Vanni M (2007) Cemento a ridosso dell'aquedotto di Alessandro Severo. Nuova Archeologia